Quantifying black carbon deposition over the Greenland ice sheet from forest fires in Canada

J. L. Thomas[1], C. M. Polashenski[2,3], A. J. Soja[4], L. Marelle[5], K. Casey[3], H. D. Choi[4], J.-C. Raut[1], C. Wiedinmyer[6], L. K. Emmons[6], J. Fast[7], J. Pelon[1], K. S. Law[1], M. G. Flanner[8], J. E. Dibb[9]

[1]LATMOS/IPSL, UPMC Univ. Paris 06 Sorbonne Universités, UVSQ, CNRS, Paris, France
[2]USACE-CRREL, Ft. Wainwright, Alaska, USA
[3]Thayer School of Engineering, Dartmouth College, Hanover, New Hampshire, USA
[4]National Institute of Aerospace, Resident at NASA Langley Research Center, 21 Langley Boulevard, Mail Stop 420, Hampton, VA 23681-2199, United States
[5]Center for International Climate and Environmental Research, Oslo, Norway
[6]National Center for Atmospheric Research, Boulder, CO, USA
[7]Pacific Northwest National Laboratory, Richland, WA, USA
[8]Department of Climate and Space Sciences and Engineering, University of Michigan, Ann Arbor, Michigan, USA
[9]Earth Systems Research Center, EOS, University of New Hampshire, Durham, New Hampshire, USA

Key Points:

- 57% of black carbon aerosol deposition in 2013 in northwest Greenland is linked to a specific event in late July/early August 2013
- Satellite observations and modeling indicate the origin of this event is emissions from forest fires burning in Canada
- Chemical transport modeling predicts the event at the right time but under-predicts black carbon deposition compared to observations

Corresponding author: J. L. Thomas, jennie.thomas@latmos.ipsl.fr
Corresponding author: J. E. Dibb, jack.dibb@unh.edu

Abstract

Black carbon (BC) concentrations observed in 22 snowpits sampled in the northwest sector of the Greenland Ice Sheet in April, 2014 have allowed us to identify a strong and widespread BC aerosol deposition event, which was dated to have accumulated in the pits from two snow storms between 27 July and 2 August, 2013. This event comprises a significant portion (57% on average across all pits) of total BC deposition over 10 months (July, 2013 – April, 2014). Here we link this deposition event to forest fires burning in Canada during summer 2013 using modeling and remote sensing tools. Aerosols were detected by both the CALIOP (onboard CALIPSO) and MODIS (Aqua) instruments during transport between Canada and Greenland. We use high-resolution regional chemical transport modeling (WRF-Chem) combined with high-resolution fire emissions (FINNv1.5) to study aerosol emissions, transport, and deposition during this event. The model captures the timing of the BC deposition event and shows fires in Canada were the main source of deposited BC. However, the model under-predicts BC deposition compared to measurements at all sites by a factor of 2–100. Under-prediction of modeled BC deposition originates from uncertainties in fire emissions and model treatment of wet removal of aerosols. Improvements in model descriptions of precipitation scavenging and emissions from wildfires are needed to correctly predict deposition, which is critical for determining the climate impacts of aerosols that originate from fires.

1 Introduction

The snow and ice of the Greenland ice sheet (GrIS) stores water with the potential to raise global sea level by approximately 7 m. In the early 2000s the ice sheet was estimated to be roughly in balance, gaining $\sim$500 Gt yr^{-1} at high elevations and losing about the same through calving and marginal melting. In recent years the ice sheet has been losing $\sim$300 Gt yr^{-1} on average, with the record breaking melt in 2012 contributing to a net loss of nearly 600 Gt [*Tedesco et al.*, 2016]. Warmer temperatures are causing outlet glaciers to thin and to move more rapidly, and a larger area of the marginal zone experiences melt for longer periods each summer. The albedo of the ice sheet has also been declining since the mid 1990s [e.g. *Tedesco et al.*, 2014, 2016].

The albedo of snow is lowered by increases in grain size and by the presence of light absorbing impurities (LAI) [*Wiscombe and Warren*, 1980], primarily black carbon (BC), mineral dust, and perhaps biological particles. BC has received a lot of attention as one of the short-lived anthropogenic climate forcers [*AMAP*, 2011, 2015] whose emissions might be quickly reduced by intentional societal action. BC in the atmosphere warms the layer in which it is transported, which may result in warming or cooling at the surface depending on the altitude of the aerosol layer and indirect impacts on cloud properties [*AMAP*, 2011; *Bond et al.*, 2013; *Flanner*, 2013]. The presence of BC in surface snow always causes reduction of albedo and heating of the snow with the magnitude of these impacts depending on concentration and season of deposition [*Hansen and Nazarenko*, 2004; *Flanner et al.*, 2007; *AMAP*, 2011, 2015; *Bond et al.*, 2013; *Ménégoz et al.*, 2013]. Climate predictions critically depend on knowledge of BC emissions, concentration and location in the troposphere, as well as the amount and location of deposition to snow and ice.

BC is a product of combustion, with strong sources from both anthropogenic activity and wildfires. In the Arctic, anthropogenic sources tend to be dominant in late winter/early spring while biomass burning is more important during summer [*McConnell et al.*, 2007; *Law et al.*, 2014]. Ice core records suggest that the anthropogenic contributions to BC decreased markedly from their peak in $\sim$1900 to 1950 and have been relatively stable since then [*McConnell et al.*, 2007]. The number and size of boreal wildfires upwind of Greenland show no significant trends since 1997 [*Tedesco et al.*, 2016], consistent with the records of fire-derived BC from Greenland ice cores [*McConnell et al.*, 2007]. It is expected that wildfires will increase markedly throughout the northern hemisphere in a warmer climate [*Stocks et al.*, 1998; *Flannigan et al.*, 2006;

Soja et al., 2007], which could enhance transport and deposition of BC to the Greenland ice sheet and accelerate melt in the future.

The likely impact of more severe wildfires on the mass balance of the Greenland ice sheet (GrIS) in the future could be estimated with models driven by future climate scenarios. However, current state of the art chemical transport models tend to poorly simulate trace gases and aerosols in the Arctic [e.g. *Eckhardt et al.*, 2015; *Emmons et al.*, 2015; *Monks et al.*, 2015]. Recent assessments have shown that concentrations of BC vary widely between models [*AMAP*, 2011, 2015].

Here, we use depth profiles of BC measured in 22 snow pits sampled during a traverse in the northwest sector of the GrIS conducted in spring 2014 [*Polashenski et al.*, 2015] to study the processes controlling BC deposition. A marked enhancement of BC and other tracers of biomass burning was observed in snow deposited in late summer 2013 in all of the pits. We refine the timing of this deposition event using detailed stratigraphy tied to weather and snow accumulation records from four autonomous weather systems deployed on a 2013 traverse [*Polashenski et al.*, 2015]. Satellite data reveals transport of smoke emissions from Canadian fires to the GrIS. A detailed high spatial resolution chemical transport model is used to: (1) quantify source fire emission from Canada; (2) transport these emissions across Canada to the GrIS; and (3) simulate the deposition of BC on the northwestern GrIS.

2 Methods

2.1 Measurements in Greenland

In this paper we focus on snowpits (Figure 1a) sampled during the SAGE (Sunlight Absorption on the Greenland Ice Sheet Experiment) surface traverse in April 2014 [*Polashenski et al.*, 2015]. All pits were sampled at 3 cm resolution from the surface to at least below the depth of the summer 2013 hoar complex, in some pits sampling extended down to summer 2012. BC concentration was determined by introducing melted samples into a single particle soot photometer (SP2) with a CETAQ ultrasonic nebulizer [*McConnell et al.*, 2007]. Further details of snow sampling and snow accumulation measurements are available in *Polashenski et al.* [2015].

2.2 Satellite observations

We use the version 4 (V4) Level 2 (L2) vertical feature mask data product (VFM) from Cloud-Aerosol LIdar with Orthogonal Polarization (CALIOP) onboard CALIPSO [*Winker et al.*, 2009]. The VFM data provides a 5-km horizontally averaged product of cloud and aerosol layers observed by the CALIOP lidar, which classifies observations as clean air, clouds, aerosols, stratospheric features, surface, subsurface, and totally attenuated backscatter (no signal). In addition, nine aerosol subtypes (clean marine, dust, polluted continental/smoke, clean continental, polluted dust, elevated smoke, dusty marine, volcanic ash and others) can also be derived from the L2 V4 aerosol layer product.

We also use the Aqua MODIS Collection 6, daily global gridded Level 3 `MYD08_D3` Dark Target Deep Blue Combined data product [*Platnick et al.*, 2015] to map aerosol optical depth (AOD) at 550 nm over the North America to Greenland domain at 1 ° by 1 ° spatial resolution. Dark Target observations with a pixel quality assessment (QA$=3$) over land, over ocean (QA>0), and high quality Deep Blue observations (QA$=2,3$) are used in creating the combined daily AOD product. Aqua MODIS data are used as it offers more stable data, with less sensor calibration degradation than the Terra MODIS instrument [*Lyapustin et al.*, 2014].

2.3 Model description and configuration

The regional model WRF-Chem version 3.5.1 [*Grell et al.*, 2005; *Fast et al.*, 2006] is used to study the influence of smoke emissions on BC deposition to the GrIS. The regional model is used with online fire emissions from FINN (version 1.5) [*Wiedinmyer et al.*, 2011] combined with fire emissions injection heights [*Grell et al.*, 2011; *Freitas et al.*, 2007], which have been evaluated for fires in Canada [*Sessions et al.*, 2011]. Aerosol physics and chemistry are described using the 8-bin Model for Simulating Aerosol Interactions and Chemistry (MOSAIC, *Zaveri et al.* [2008]), assuming internally mixed aerosols and volume-averaged optical properties and hygroscopicity within each bin. Interstitial and cloud-borne aerosols are tracked explicitly: aerosols can be activated in liquid clouds [*Abdul-Razzak and Ghan*, 2000, 2002], and later removed or re-suspended. Wet removal occurs when droplets containing aerosols are converted to precipitation. Precipitation also removes aerosols by impaction. In our study, aerosol-cloud interactions are included in both resolved and parameterized clouds [*Chapman et al.*, 2009; *Berg et al.*, 2015]. Additional details of the model setup are provided in the electronic supplement (Figures S1-S3, Table S1). The model simulation timeframe and domain were chosen using the Lagrangian particle dispersion model FLEXPART-WRF [*Brioude et al.*, 2013] combined with fires detected by MODIS between 17-28 July 2013 (Figure 2 and Figures S4 and S5). An example FLEXPART-WRF run backwards to identify source fires for pit B1-B is shown in Figure 2b. Here we trace air backwards for 10 days (release on 1 Aug 2013) to identify source fires primarily in Québec with some contribution from fires farther east in Canada. To study BC emissions, processing, and deposition we perform three model runs from 17 July 2013 – 5 August 2013. First, a BASE run with all emissions included. Second, a NOFIRE run, which is the same as the BASE run, but excludes fire emissions within the model domain. Third, a 2xBC run, which is the same as the BASE run with BC emissions from fires within the domain increased by a factor of two.

3 Results and Discussion

3.1 A prominent BC deposition event in 2013

In snow layers that were deposited from 2012 – 2014 in NW Greenland, one widespread BC deposition event was observed [*Polashenski et al.*, 2015]. This BC rich layer was found during 2014 sampling in a stratigraphic layer that had been deposited during the summer of 2013 and had peak BC concentrations ranging from 2.8–43 ng/g (ng BC per gram of snowmelt, 15 ng/g average). Within the BC rich layer, concentrations above 3 ng/g were strongly correlated with elevated concentrations of NH_4 [*Polashenski et al.*, 2015], indicating the enhanced BC was likely biomass burning-derived [see review of *Legrand et al.*, 2016]. Radiative transfer modeling showed the layer was sufficiently contaminated with BC to have an impact on surface albedo [*Polashenski et al.*, 2015]. Snow accumulation sensors on automatic weather stations, however, indicated the layer was buried by heavy snowfall shortly after its deposition and likely did not impact the ice sheet energy balance over a sustained time period. We note that similar deposition events under other circumstances could have substantial impacts on ice sheet energy balance.

A prominent hoar complex present in all pits is used as an isochron across the study region. The four weather stations deployed in the region recorded no snow accumulation during 10 – 26 July, and air temperature sensors recorded substantial ($\sim$10 °C) diurnal temperature variation 14 – 26 July typical of summer surface hoar formation events. This hoar layer developed during July just beneath the surface and the top of this layer closely represents the location of the snow surface from 10 – 27 July.

Snow accumulation sensors show three snow accumulation events on 27 – 28 July, 29 July, and 1 – 2 August, totaling 0.1–0.25 m accumulation at the sites. Larger snowfall followed on 11 – 13 and 17 –19 August, totaling $\sim$0.1–0.4 m accumulation across the sites. These snow accumulation events were discernible as two distinct stratigraphic layers in all pits, and

up to 5 in some. In pits where the 27 July – 2 August snowfalls were preserved as three separate layers, elevated BC was present in the first and third layers, representing snow that fell on 27 – 28 July and 1 – 2 August. In pits where wind redistribution mixed thin layers, elevated BC was found in snow deposited 27 July to 2 August and not the larger mid August layers. The unique circumstance of the high BC layer being deposited directly atop the summer hoar layer allowed us to extrapolate the dating of the snowfall events from the weather station sites to other snow pits with high confidence.

Depth profiles of BC concentrations in all snowpits are shown with a pair of red lines bounding the layers that accumulated 27 July – 2 August (Figure 1b). BC values are normalized by dividing the concentration in each sample by the maximum concentration measured in that pit profile. Enhanced BC concentrations are apparent between the red lines as warmer colors. Integrated BC deposition from 27 July – 2 August is compared to BC deposition integrated from the summer 2013 hoar layer to the snow surface in each pit (Figure 1c). In several of the pits, BC deposited in this short interval represents a dominant fraction of the total BC accumulation between summer 2013 and the time of sampling in April 2014. In all pits, these storms delivered a significant fraction (average 57%) of the 9–10 month total (Figure 1c).

3.2 Satellite observations of aerosols linked to the 27 July – 2 August 2013 deposition event

Large smoke plumes containing elevated aerosols were identified in the CALIOP VFM data between Canada and Greenland in late July and early August 2013. One example VFM is shown in Figure 3a for 28 July 2013. CALIOP detected primarily thick clouds over Greenland, with the signal attenuated below 5 km north of 65 °N. South of this, CALIOP detected a large aerosol plume extending from 51 °N – 65 °N (Figure 3a) from the surface up to 4 km. We note that this plume was primarily identified as an elevated smoke layer or polluted continental/smoke layer in the aerosol subtype derived as part of the L2 V4 aerosol layer product (magenta box in Figure S6).

Daily 550 nm AOD maps from MODIS in late July show values greater than 0.8 over the Canadian source fires (Figure 4a) and a smoke plume with AOD $\sim$0.4 over the Davis Strait (Figure 4b). AOD is not reported in large portions of the fire source regions (fire detections shown in Figure 2, daily maps in Figure S7) due to thick smoke and clouds preventing AOD measurements. Specifically, large fires were detected in Québec and western Canada where AOD measurements are not reported. Thick clouds over Baffin Bay associated with the storm system that uplifted aerosols and advected them over the northwest region of Greenland prevented MODIS retrievals of AOD during the final stage of transport to our sampling locations on the GrIS. The CALIPSO track on 28 July 2013 (see Figure 3a) is shown on the MODIS AOD figure for 28 July (Figure 4b). The CALIOP measurements are co-located with the large AOD maximum seen in MODIS data near 61 °N, 92 °W. A dense elevated smoke plume is identified at this location (Figure S6), co-located with some clouds. For this plume, the depolarization and color ratios are more typical of aerosols and the CALIOP algorithm may be mis-identifying aerosols as clouds (e.g. clouds detected at 60.7 °N at an altitude of 3 km, Figure 3a).

3.3 Model representation of the 26 July – 2 August deposition event

WRF-Chem predicted PM2.5 (particulate matter with a diameter of less than 2.5 μm) and BC along the CALIPSO track shown in Figure 3a show strong enhancements at the same location and altitudes as the smoke plume observed by the CALIOP lidar (Figure 3c and 3e). In the model grid cells along this track comparing the BASE and NOFIRES simulations indicate that between 40% and 100% of PM 2.5 mass was contributed by the fire emissions (Figure 3d). Between 80 to 100% of the BC in the modeled plume can be attributed to fire emissions (Figure 3f).

Model predicted 550 nm AOD is compared with MODIS Aqua AOD observations in Figure 4. In the fire source region, AOD measurements are limited, but some AOD values are reported close to the fires. Where comparisons can be made, for example in northern Canada on 26 July, the model under-predicts measured AOD close to the fires. During transport towards the GrIS, aerosols are seen over Hudson Bay by MODIS on 28 July 2013 (note they were also seen on this day by CALIPSO, Figure 3). MODIS AOD is also higher than the WRF Chem predictions here. We suggest that low modeled AOD upwind of Greenland is due to under-predicted aerosol emissions from fires, which have uncertainties of a factor of 2 or higher [e.g. *Wiedinmyer et al.*, 2006, 2011; *Turquety et al.*, 2014]. The FINNv1.5 fire emissions are driven by fire detections from MODIS (daily fire maps in Figure S7). Missed detections often result from aerosols and clouds obscuring the MODIS measurements, particularly for big fires, leading to under-prediction of the emissions.

Aerosol transport from fires in Canada to Greenland during our study period (see AOD in Figure S8) corresponds to two main modeled BC deposition events, via primarily wet deposition that occurs along with precipitation on 26 July 2013 and 31 July - 1 August 2013 (Figure 5a). Note that modeled aerosol deposition for this event begins on 26 July, while measured deposition was dated to 27 July. In order to capture the entire event in the model, we use model predicted deposition starting on 26 July (00:00 UTC) through 2 August (00:00 UTC) to compare with measurements. We track BC deposition as the sum of all cloud-borne BC that is lost to precipitation (rain, snow, graupel, and ice) and removal of BC by impaction with all phases of precipitation. Modeled BC deposition is calculated as the sum of in-cloud scavenging of activated aerosols by conversion to precipitation, and below-cloud scavenging by impaction. We calculate the contribution from fires to BC deposition (using the difference between the BASE and NOFIRE runs as in Figure 3) and find that the first, smaller BC deposition event (26 July) does not predominantly originate from fires within the model domain (Figure 5b), rather, the deposited BC comes from outside the regional model domain or anthropogenic emissions within the model domain. The second event on 31 July – 1 August 2013 deposits aerosols that are mainly of fire origin (between 60–100 % of BC deposited). We note that these events cannot reliably be separated in the snow pit sampling (discussed above) due to wind redistribution of snow deposited between 27 July – 2 August in some pits.

WRF-Chem captures the timing of the measured deposition events, however the average modeled deposition (32.8 $\mu g\ m^{-2}$) is an order of magnitude lower than the average measured deposition in the 22 pits (352.9 $\mu g\ m^{-2}$) (see Table S2). The best agreement (50 % underestimate by the model) is found for pit locations close to the coast and at lower elevations. The observed deposition increases much more strongly with altitude and distance inland than the model predicts. In the pits with strongest measured BC deposition, model predictions are more than a factor of 100 too low (Table S2). Wet deposition represents 99 % of the total model predicted BC deposition in all pits during the main deposition event (26 July – 3 August 2013) and 93.9 % of total deposition within the model domain (from 20 July 2013 – 3 Aug 2013). We have completed a sensitivity run with the emissions of BC from fires multiplied by a factor of two, which results in improved BC deposition values at coastal sites, but similar under prediction of BC inland (Table S2). To explore if model disagreement is due to incorrect prediction of precipitation events during this period, we compared the model predicted total precipitation with the precipitation rates inferred from pits (Table S2) and compare model predictions to the Global Precipitation Climatology Project (GPCP v1.2) daily precipitation product (Figure S9). We find that the model captures 77% of observed precipitation in pits and the general patterns of precipitation reported by GPCP, suggesting that imperfections in modeled meteorology alone cannot explain the large differences in BC deposition rates.

Modeled aerosols in the lowest portion of the troposphere are, in general, scavenged prior to arriving at the center of the GrIS. We have calculated time averaged vertical profiles of BC aerosols over all 22 pits (Figure S10), which show that aerosol concentrations in the lower troposphere over the GrIS (below 4 km) in the model are nearly completely depleted during the main deposition event (31 July and 1 Aug). Recent aircraft observations near northern Nor-

way and farther north into the Arctic [*Roiger et al.*, 2015; *Schwarz et al.*, 2017], found that BC concentrations generally remained above 5 ng kg^{-1} during a very rainy/stormy portion of July 2012. BC vertical profiles extracted from the model have low BC concentrations in the lower troposphere over pits compared to earlier in the simulation, near the fire source region and the CALIPSO overpass between Canada and Greenland. This provides evidence that aerosol scavenging occurs in the model prior to the storm event reaching the plateau of the Greenland ice sheet.

Despite significant progress on the representation of aerosol-cloud interactions in WRF-Chem [*Chapman et al.*, 2009; *Berg et al.*, 2015], explicit treatment of aerosols as ice nuclei is not yet included. Rather, the main removal mechanism currently in the model is uptake of aerosols into existing liquid cloud droplets by wet scavenging and by impaction with precipitation. There is evidence that BC can be enriched in mixed phase clouds and that BC serves as an efficient ice nuclei under certain conditions [*DeMott et al.*, 1999, 2009; *Cozic et al.*, 2008; *Petters et al.*, 2009]. The role aerosols from biomass burning emissions play in ice nucleation and uptake to mixed phase clouds are open research questions, which are important to address in order to improve predicted aerosol deposition in models in the future. In addition, improved knowledge of BC removal processes near the source region and along transport pathways have been identified as a key uncertainty for modeling BC in remote environments [e.g. *Shen et al.*, 2014].

A combination of factors result in poor quantitive agreement with measured BC deposition rates. First, uncertainties and errors in the magnitude and vertical extent of fire emissions impact the results, as highlighted by the comparison between the model predicted AOD and MODIS AOD. Second, we suggest that imperfect representation of scavenging of aerosols by clouds is an important area for model improvement in the future. Third, aerosols are deposited in the model too early, resulting in low deposition rates in the interior of the GrIS. This can be due to incomplete representation of scavenging processes in the model, which combined with low emissions, result in low BC deposition rates. In order to provide detailed information needed for specific model improvements, there is a need for simultaneous monitoring of fresh emissions, atmospheric measurements during transport, and measurements of deposition to disentangle these complex processes.

4 Conclusions

We have shown that wet deposition of a wildfire smoke plume in a series of storms during a week in late July – August 2013 accounted for nearly 60% of the BC accumulating in the snow in northwest Greenland over 10 months (July 2013 – April 2014). Fire hotspot detection and AOD maps from MODIS established a qualitative link between the smoke reaching Greenland and fires burning in western Canada which was strengthened by observations of the smoke plume by CALIOP during transport in route to Greenland. Simulations with the regional chemical transport model WRF-Chem reproduce the smoke plume observed by MODIS and CALIOP during transport and the model predicts significant BC deposition that occurs during two precipitation events on 26 July and 31 July – 1 August, which agrees with the timing of measured BC deposition. However, BC deposition in the model is underpredicted compared to measurements by an order of magnitude (averaged over the 22 pits in this study). The underprediction of BC increases from a factor of 2 at the lowest/warmest pit sites to a factor of 100 at pits higher on the GrIS and further from the coast. This gradient suggests that the model may be scavenging BC too efficiently in warm clouds and/or not efficiently enough in cold clouds. The under-prediction of BC deposition even at the lower altitude snowpits indicate that the smoke plume reaching Greenland in the model was less significant than the actual plume, likely due to a combination of underestimated emissions from the source fires and unrealistically rapid removal of BC during transport. This study suggests that WRF-Chem predicts the transport of smoke from boreal fires over regional and continental scales, but improvements in model treatment of precipitation scavenging and emissions from wildfires are needed if these models are to be used to predict the climate impacts of smoke in the Arctic.

5 Figures

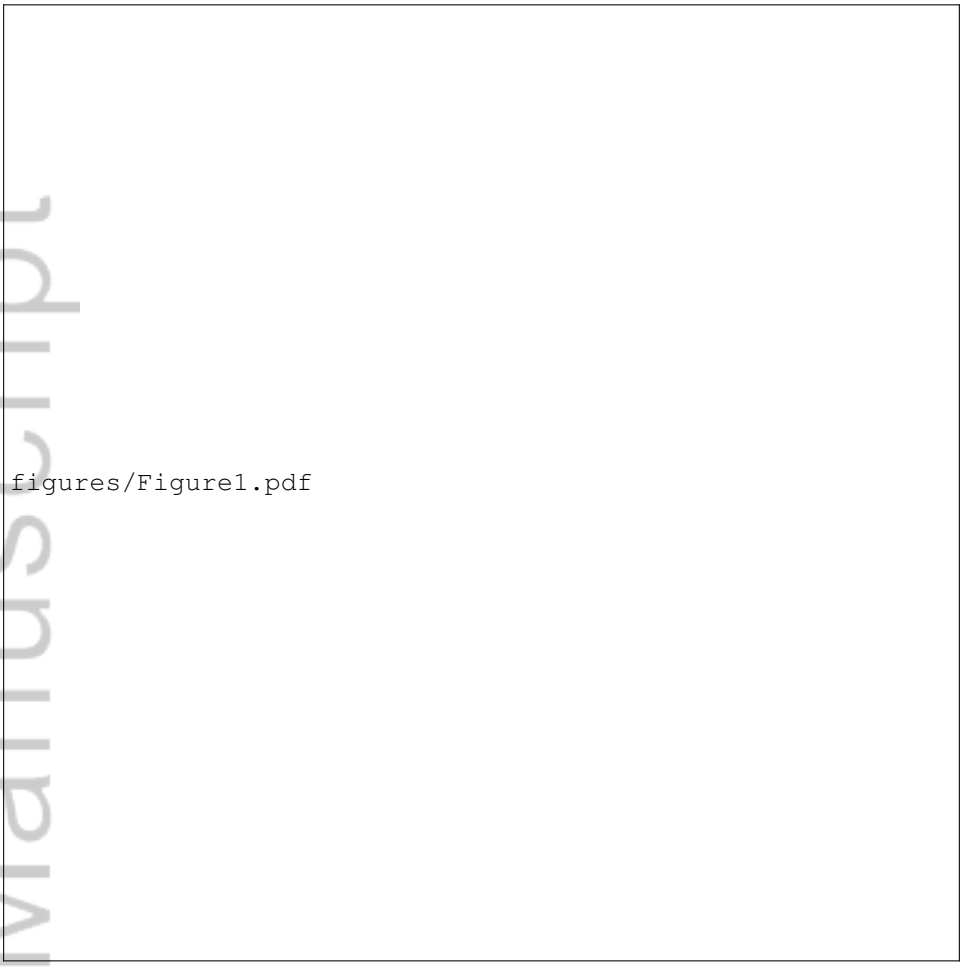

Figure 1. (a) Locations of sampling snowpit sites in NW Greenland, (b) Plot of normalized BC concentration observed in the pits, with the mid-July 2013 hoar/melt layer set to 0 cm. Red lines highlight the boundaries of stratigraphic layers interpreted from physical stratigraphy and weather station accumulation sensors to have accumulated during the 27 July – 2 August storm sequence (high BC layers are substantially concentrated in these layers). BC concentrations are normalized by the peak value in each pit for comparison during this event because the magnitude of the peak deposition varies substantially between pits. (c) A plot of the BC accumulation during the 27 July to 2 August. event, and the cumulative BC accumulation between mid July 2013 and our sampling dates in April 2014.

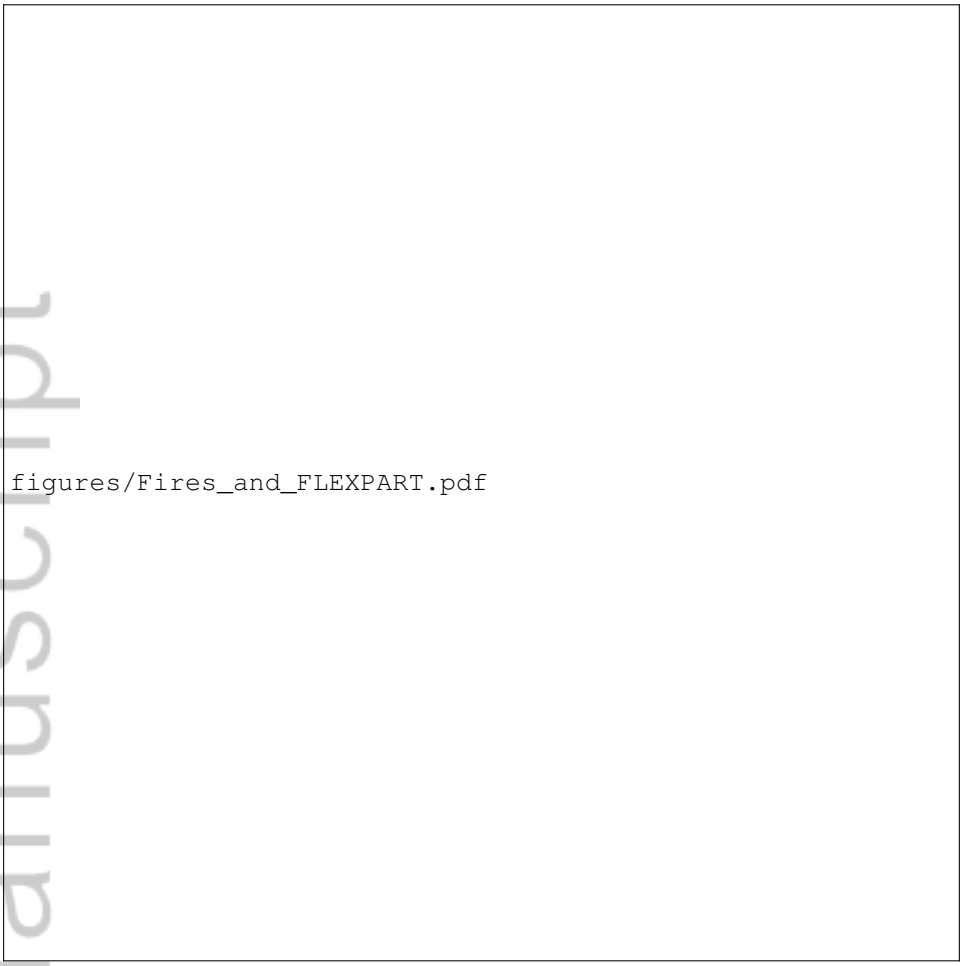

Figure 2. (a) NASA Fire Information for Resource Management System (FIRMS) fire detections on 17-28 July 2013. The point size proportional to the log of the fire radiative power, three example point sizes with the corresponding FRP are shown as a reference. FIRMS data are described in *Kaufman et al.* [1998], *Wooster et al.* [2005], and *Giglio et al.* [2016]. (b) FLEXPART-WRF total column integrated (10 day) Potential Emissions Sensitivity (PES). PES values are shown in seconds, which represent the residence time of particles as a function of location for the 10 day airmass history. Results are shown for particles released at the location of the B1-B pit from 1 August 00:00 UTC - 2 August 00:00 UTC between 1-5 km (AGL). FLEXPART-WRF is driven by WRF-Chem predicted meteorology (BASE run). All pit locations are shown in purple and the B1-B pit location is shown by the large magenta dot. The plume centroid locations 1-7 days prior to release are also shown (white box, black number).

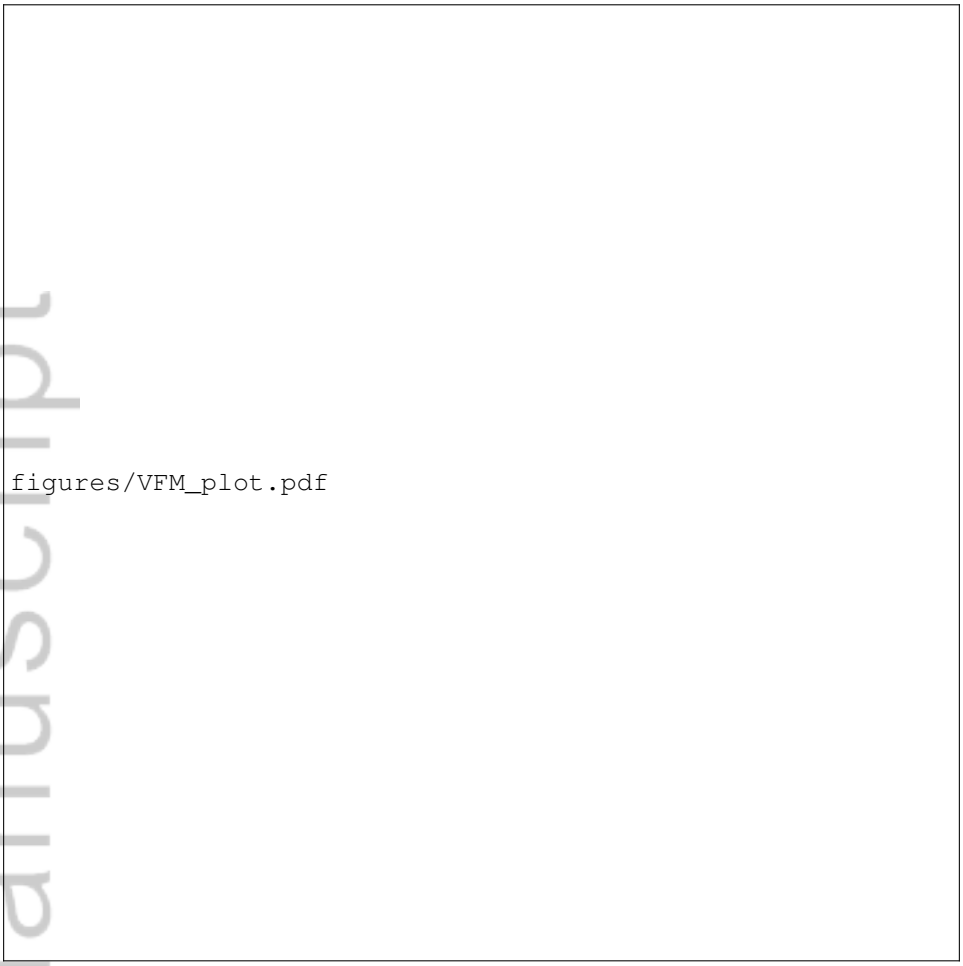

Figure 3. Vertical feature mask (VFM) shown in panel (a) from the CALIPSO overpass on 28 July 2013 (8:44 UTC – 8:52 UTC), overpass location shown in panel (b). Note that the VFM shows clouds (teal) and aerosols (blue). WRF-Chem model results were extracted along the overpass (red portion panel (b)) on 28 July 2013 (9:00 UTC) in panels (c)–(f). PM 2.5 is shown in (c) and BC is shown in (e) for the BASE run. The percent contribution from fires within the WRF-Chem domain to PM 2.5 and BC is shown in (d) and (f).

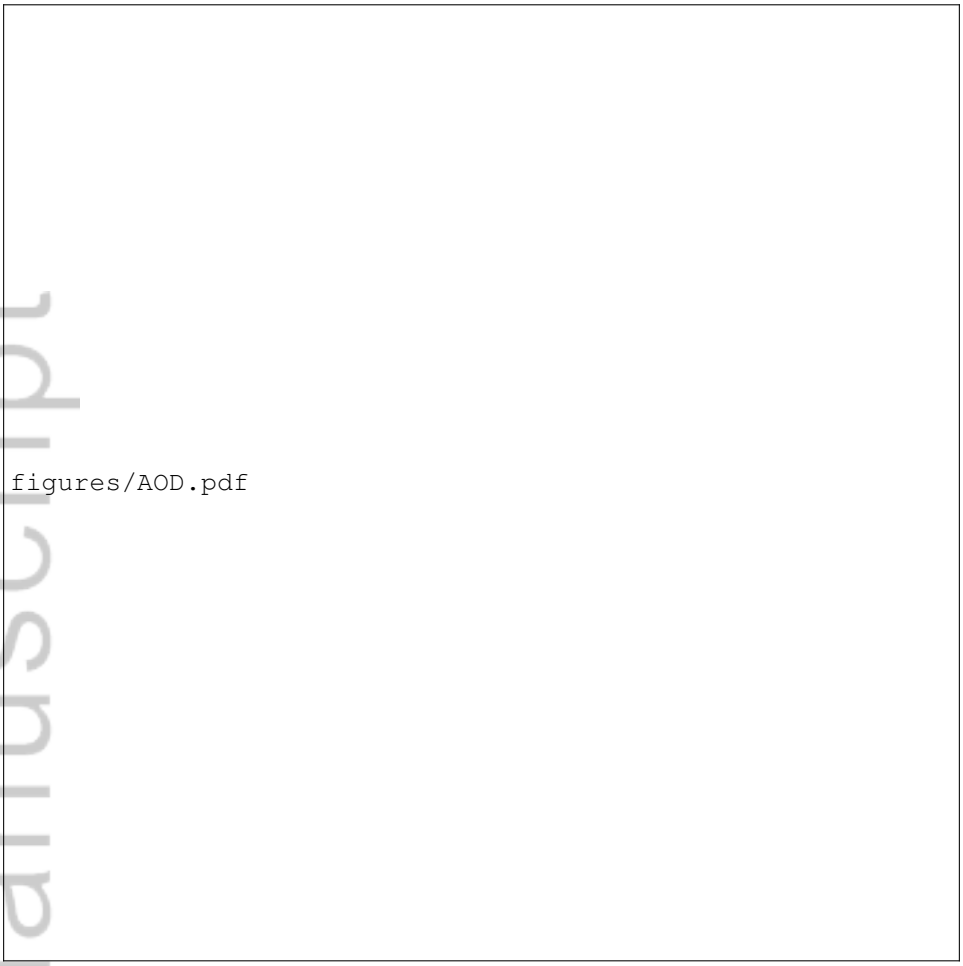

Figure 4. 550 nm AOD on 26, 28, and 30 July 2013 from MODIS Aqua (00:00–23:59 UTC) (panels a–c) compared to WRF-Chem results at 12:00 UTC on the same days (panels d–f). On 28 July 2013 the CALIPSO overpass is shown in grey and teal, the teal portion of the overpass indicates the data used in Figure 3.

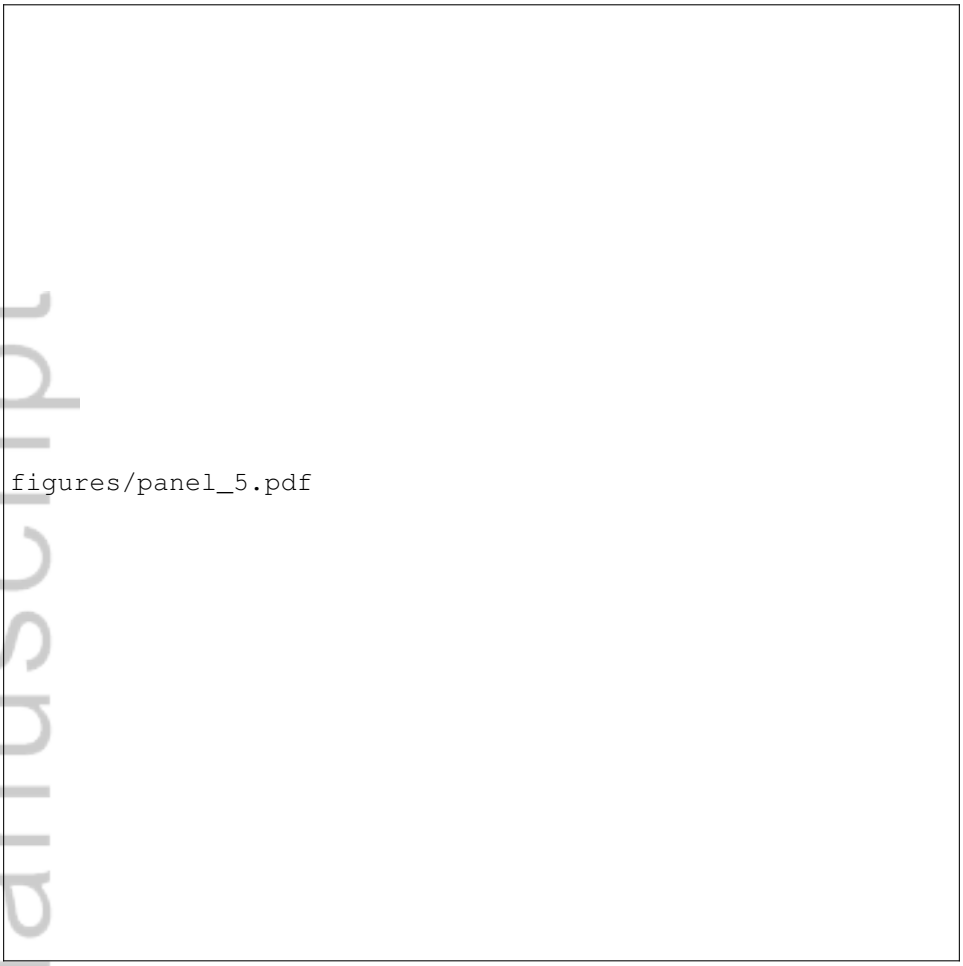

Figure 5. Hourly BC deposition (sum of wet and dry deposition) in μg/m^2/h for the pits in Fig. 1 predicted by the WRF-Chem BASE run (a) and percent contribution of BC deposition to fires within the model domain (b).

Acknowledgments

The SAGE traverses were supported by National Science Foundation Division of Polar Program awards ARC1203876 and ARC1204145 to UNH and CRREL, respectively. Successful execution of these ambitious sampling campaigns would not have been possible without the excellent logistic support provided by CPS, and airlift by the NY 109th ANG. We also deeply appreciate the capable assistance field party members Michael and Nathan Stewart, Lauren Farnsworth, and Carolyn Stwertka provided to traverse leader CMP. The focus of the NSF project was surface albedo and the factors controlling it over space and time. Collection of deeper profiles in all of the SAGE pits and analysis of the returned samples was made possible by support from NASA's Interdisciplinary Research in Earth Science Program (awards NNX14AE72G to UNH and NNH15AZ74I to CRREL). Data analysis and interpretation for this paper by CMP, AJS, KC, HDC, MGF, and JED were primarily supported by NASA. In addition, analyses used in this study were produced with the Giovanni online data system, developed and maintained by the NASA GES DISC. We acknowledge the MODIS and CALIOP mission scientists and associated NASA and CNES personnel for the production of the data used in this research effort. We also acknowledge the use of data and imagery from LANCE FIRMS operated by the NASA/GSFC/Earth Science Data and Information System (ESDIS) with funding provided by NASA/HQ. Work at the National Center for Atmospheric Research (performed by CW and LE) is sponsored by the National Science Foundation. We thank the large community of FLEXPART-WRF and WRF-Chem developers including the Atmospheric Chemistry Observations and Modeling Lab (ACOM) of NCAR for developing the WRF-Chem preprocessor tools. We specifically thank R. Easter and L. Berg for helpful discussions regarding WRF-Chem. We acknowledge T. Onishi for technical support with running WRF-Chem. We also thank the French CA project PARCS for funding. The WRF-Chem and FLEXPART-WRF models are publicly available, the WRF-Chem code used in this study is available by contacting L. Marelle. Satellite observations used in this study are publicly available online from NASA. Snowpit data are archived at `https://arcticdata.io`, doi:10.18739/A2NQ09. Computing resources were provided by IDRIS HPC resources by the GENCI allocation 2016-017141 and by the IPSL mesoscale computing center (Calcul Intensif pour le Climat, l'Atmosphère et la Dynamique).

6 References

References

Abdul-Razzak, H., and S. J. Ghan (2000), A parameterization of aerosol activation: 2. multiple aerosol types, *J. Geophys. Res. Atmos.*, *105*(D5), 6837–6844.

Abdul-Razzak, H., and S. J. Ghan (2002), A parameterization of aerosol activation 3. sectional representation, *J. Geophys. Res. Atmos.*, *107*(D3).

AMAP (2011), *The Impact of Black Carbon on Arctic Climate*, AMAP, Oslo, Norway.

AMAP (2015), *AMAP Assessment 2015: Black carbon and ozone as Arctic climate forcers*, AMAP, Oslo, Norway.

Berg, L., M. Shrivastava, R. Easter, J. Fast, E. Chapman, Y. Liu, and R. Ferrare (2015), A new WRF-Chem treatment for studying regional-scale impacts of cloud processes on aerosol and trace gases in parameterized cumuli, *Geosci. Model Dev.*, *8*(2), 409–429.

Bond, T. C., S. J. Doherty, D. Fahey, P. Forster, T. Berntsen, B. DeAngelo, M. Flanner, S. Ghan, B. Kärcher, D. Koch, et al. (2013), Bounding the role of black carbon in the climate system: A scientific assessment, *J. Geophys. Res. Atmos.*, *118*(11), 5380–5552.

Brioude, J., D. Arnold, A. Stohl, M. Cassiani, D. Morton, P. Seibert, W. Angevine, S. Evan, A. Dingwell, J. D. Fast, et al. (2013), The Lagrangian particle dispersion model FLEXPART-WRF version 3.1, *Geosci. Model Dev.*, *6*(6), 1889–1904.

Chapman, E. G., W. Gustafson Jr, R. C. Easter, J. C. Barnard, S. J. Ghan, M. S. Pekour, and J. D. Fast (2009), Coupling aerosol-cloud-radiative processes in the WRF-Chem model: Investigating the radiative impact of elevated point sources, *Atmos. Chem. Phys.*, *9*(3), 945–964.

Cozic, J., S. Mertes, B. Verheggen, D. J. Cziczo, S. Gallavardin, S. Walter, U. Baltensperger, and E. Weingartner (2008), Black carbon enrichment in atmospheric ice particle residuals observed in lower tropospheric mixed phase clouds, *J. Geophys. Res. Atmos.*, *113*(D15).

DeMott, P., Y. Chen, S. Kreidenweis, D. Rogers, and D. E. Sherman (1999), Ice formation by black carbon particles, *Geophys. Res. Lett.*, *26*(16), 2429–2432.

DeMott, P. J., M. D. Petters, A. J. Prenni, C. M. Carrico, S. M. Kreidenweis, J. L. Collett, and H. Moosmüller (2009), Ice nucleation behavior of biomass combustion particles at cirrus temperatures, *J. Geophys. Res. Atmos.*, *114*(D16).

Eckhardt, S., B. Quennehen, D. J. L. Olivié, T. K. Berntsen, R. Cherian, J. H. Christensen, W. Collins, S. Crepinsek, N. Daskalakis, M. Flanner, A. Herber, C. Heyes, Ø. Hodnebrog, L. Huang, M. Kanakidou, Z. Klimont, J. Langner, K. S. Law, M. T. Lund, R. Mahmood, A. Massling, S. Myriokefalitakis, I. E. Nielsen, J. K. Nøjgaard, J. Quaas, P. K. Quinn, J.-C. Raut, S. T. Rumbold, M. Schulz, S. Sharma, R. B. Skeie, H. Skov, T. Uttal, K. von Salzen, and A. Stohl (2015), Current model capabilities for simulating black carbon and sulfate concentrations in the Arctic atmosphere: a multi-model evaluation using a comprehensive measurement data set, *Atmos. Chem. Phys.*, *15*(16), 9413–9433.

Emmons, L. K., S. R. Arnold, S. A. Monks, V. Huijnen, S. Tilmes, K. S. Law, J. L. Thomas, J.-C. Raut, I. Bouarar, S. Turquety, Y. Long, B. Duncan, S. Steenrod, S. Strode, J. Flemming, J. Mao, J. Langner, A. M. Thompson, D. Tarasick, E. C. Apel, D. R. Blake, R. C. Cohen, J. Dibb, G. S. Diskin, A. Fried, S. R. Hall, L. G. Huey, A. J. Weinheimer, A. Wisthaler, T. Mikoviny, J. Nowak, J. Peischl, J. M. Roberts, T. Ryerson, C. Warneke, and D. Helmig (2015), The POLARCAT Model Intercomparison Project (POLMIP): overview and evaluation with observations, *Atmos. Chem. Phys.*, *15*(12), 6721–6744.

Fast, J. D., W. I. Gustafson, R. C. Easter, R. A. Zaveri, J. C. Barnard, E. G. Chapman, G. A. Grell, and S. E. Peckham (2006), Evolution of ozone, particulates, and aerosol direct radiative forcing in the vicinity of houston using a fully coupled meteorology-chemistry-aerosol model, *J. Geophys. Res. Atmos.*, *111*(D21).

Flanner, M. G. (2013), Arctic climate sensitivity to local black carbon, *J. Geophys. Res. Atmos.*, *118*(4), 1840–1851.

Flanner, M. G., C. S. Zender, J. T. Randerson, and P. J. Rasch (2007), Present-day climate forcing and response from black carbon in snow, *J. Geophys. Res. Atmos.*, *112*(D11).

Flannigan, M. D., B. J. Stocks, and M. G. Weber (2006), *Fire and climatic change in temperate ecosystems of the western Americas*, vol. 160, chap. Fire regimes and climatic change in Canadian forests, Springer.

Freitas, S. R., K. M. Longo, R. Chatfield, D. Latham, M. Silva Dias, M. Andreae, E. Prins, J. Santos, R. Gielow, and J. Carvalho Jr (2007), Including the sub-grid scale plume rise of vegetation fires in low resolution atmospheric transport models, *Atmos. Chem. Phys.*, *7*(13), 3385–3398.

Giglio, L., W. Schroeder, and C. O. Justice (2016), The collection 6 MODIS active fire detection algorithm and fire products, *Remote Sens. Environ.*, *178*, 31–41.

Grell, G., S. R. Freitas, M. Stuefer, and J. Fast (2011), Inclusion of biomass burning in WRF-Chem: impact of wildfires on weather forecasts, *Atmos. Chem. Phys.*, *11*(11), 5289–5303.

Grell, G. A., S. E. Peckham, R. Schmitz, S. A. McKeen, G. Frost, W. C. Skamarock, and B. Eder (2005), Fully coupled "online" chemistry within the WRF model, *Atmos. Env.*, *39*(37), 6957–6975.

Hansen, J., and L. Nazarenko (2004), Soot climate forcing via snow and ice albedos, *Proc. Natl. Acad. Sci. USA*, *101*(2), 423–428.

Kaufman, Y. J., C. O. Justice, L. P. Flynn, J. D. Kendall, E. M. Prins, L. Giglio, D. E. Ward, W. P. Menzel, and A. W. Setzer (1998), Potential global fire monitoring from eos-modis, *J. Geophys. Res. Atmos.*, *103*(D24), 32,215–32,238.

Law, K. S., A. Stohl, P. K. Quinn, C. A. Brock, J. F. Burkhart, J.-D. Paris, G. Ancellet, H. B. Singh, A. Roiger, H. Schlager, et al. (2014), Arctic air pollution: new insights from POLARCAT-IPY, *Bull. Am. Meteorol. Soc.*, *95*(12), 1873–1895.

Legrand, M., J. McConnell, H. Fischer, E. W. Wolff, S. Preunkert, M. Arienzo, N. Chellman, D. Leuenberger, O. Maselli, P. Place, M. Sigl, S. Schüpbach, and M. Flannigan (2016), Boreal fire records in northern hemisphere ice cores: a review, *Clim. Past*, *12*(10), 2033–2059.

Lyapustin, A., Y. Wang, X. Xiong, G. Meister, S. Platnick, R. Levy, B. Franz, S. Korkin, T. Hilker, J. Tucker, F. Hall, P. Sellers, A. Wu, and A. Angal (2014), Scientific impact of MODIS C5 calibration degradation and C6+ improvements, *Atmos. Meas. Tech.*, *7*(12), 4353–4365.

McConnell, J. R., R. Edwards, G. L. Kok, M. G. Flanner, C. S. Zender, E. S. Saltzman, J. R. Banta, D. R. Pasteris, M. M. Carter, and J. D. Kahl (2007), 20th-century industrial black carbon emissions altered Arctic climate forcing, *Science*, *317*(5843), 1381–1384.

Ménégoz, M., G. Krinner, Y. Balkanski, A. Cozic, O. Boucher, and P. Ciais (2013), Boreal and temperate snow cover variations induced by black carbon emissions in the middle of the 21st century, *The Cryosphere*, *7*(2), 537–554.

Monks, S. A., S. R. Arnold, L. K. Emmons, K. S. Law, S. Turquety, B. N. Duncan, J. Flemming, V. Huijnen, S. Tilmes, J. Langner, J. Mao, Y. Long, J. L. Thomas, S. D. Steenrod, J. C. Raut, C. Wilson, M. P. Chipperfield, G. S. Diskin, A. Weinheimer, H. Schlager, and G. Ancellet (2015), Multi-model study of chemical and physical controls on transport of anthropogenic and biomass burning pollution to the Arctic, *Atmos. Chem. Phys.*, *15*(6), 3575–3603.

Petters, M. D., M. T. Parsons, A. J. Prenni, P. J. DeMott, S. M. Kreidenweis, C. M. Carrico, A. P. Sullivan, G. R. McMeeking, E. Levin, C. E. Wold, et al. (2009), Ice nuclei emissions from biomass burning, *J. Geophys. Res. Atmos.*, *114*(D7).

Platnick, S., P. Hubanks, K. Meyer, and M. D. King (2015), *MODIS Atmosphere L3 Monthly Product (08_L3)*, chap. NASA MODIS Adaptive Processing System, Goddard Space Flight Center.

Polashenski, C. M., J. E. Dibb, M. G. Flanner, J. Y. Chen, Z. R. Courville, A. M. Lai, J. J. Schauer, M. M. Shafer, and M. Bergin (2015), Neither dust nor black carbon causing apparent albedo decline in Greenland's dry snow zone: Implications for modis C5 surface reflectance, *Geophys. Res. Lett.*, *42*(21), 9319–9327, 2015GL065912.

Roiger, A., J.-L. Thomas, H. Schlager, K. S. Law, J. Kim, A. Schäfler, B. Weinzierl, F. Dahlkötter, I. Krisch, L. Marelle, A. Minikin, J.-C. Raut, A. Reiter, M. Rose, M. Scheibe, P. Stock, R. Baumann, I. Bouarar, C. Clerbaux, M. George, T. Onishi, and J. Flemming (2015), Quantifying emerging local anthropogenic emissions in the Arctic region: The ACCESS aircraft campaign experiment, *Bull. Am. Meteorol. Soc.*, *96*(3), 441–460.

Schwarz, J. P., B. Weinzierl, B. H. Samset, M. Dollner, K. Heimerl, M. Z. Markovic, A. E. Perring, and L. Ziemba (2017), Aircraft measurements of black carbon vertical profiles show upper tropospheric variability and stability, *Geophys. Res. Lett.*, *44*, 1132—1140.

Sessions, W., H. Fuelberg, R. Kahn, and D. Winker (2011), An investigation of methods for injecting emissions from boreal wildfires using WRF-Chem during arctas, *Atmos. Chem. Phys.*, *11*(12), 5719–5744.

Shen, Z., J. Liu, L. W. Horowitz, D. K. Henze, S. Fan, L. I. H., D. L. Mauzerall, J.-T. Lin, and S. Tao (2014), Analysis of transpacific transport of black carbon during hippo-3: implications for black carbon aging, *Atmos. Chem. Phys.*, *14*(12), 6315–6327.

Soja, A. J., N. M. Tchebakova, N. H. French, M. D. Flannigan, H. H. Shugart, B. J. Stocks, A. I. Sukhinin, E. Parfenova, F. S. Chapin, and P. W. Stackhouse (2007), Climate-induced boreal forest change: predictions versus current observations, *Glob. Planet. Change*, *56*(3), 274–296.

Stocks, B. J., M. Fosberg, T. Lynham, L. Mearns, B. Wotton, Q. Yang, J. Jin, K. Lawrence, G. Hartley, J. Mason, et al. (1998), Climate change and forest fire potential in Russian and Canadian boreal forests, *Climatic change*, *38*(1), 1–13.

Tedesco, M., J. Box, J. Cappelen, X. Fettweis, T. Mote, R. van de Wal, C. Smeets, and J. Wahr (2014), Greenland ice sheet, *NOAA Arctic Report Card*, p. 22.

Tedesco, M., S. Doherty, X. Fettweis, P. Alexander, J. Jeyaratnam, and J. Stroeve (2016), The darkening of the Greenland ice sheet: trends, drivers, and projections (1981–2100), *The Cryosphere*, *10*(2), 477–496.

Turquety, S., L. Menut, B. Bessagnet, A. Anav, N. Viovy, F. Maignan, and M. Wooster (2014), APIFLAME v1.0: high-resolution fire emission model and application to the Euro-Mediterranean region, *Geosci. Model Dev.*, *7*(2), 587–612.

Wiedinmyer, C., B. Quayle, C. Geron, A. Belote, D. McKenzie, X. Zhang, S. O'Neill, and K. K. Wynne (2006), Estimating emissions from fires in North America for air quality modeling, *Atmos. Env.*, *40*(19), 3419–3432.

Wiedinmyer, C., S. Akagi, R. J. Yokelson, L. Emmons, J. Al-Saadi, J. Orlando, and A. Soja (2011), The Fire INventory from NCAR (FINN): a high resolution global model to estimate the emissions from open burning, *Geosci. Model Dev.*, *4*, 625.

Winker, D. M., M. A. Vaughan, A. Omar, Y. Hu, K. A. Powell, Z. Liu, W. H. Hunt, and S. A. Young (2009), Overview of the CALIPSO mission and CALIOP data processing algorithms, *J. Atmos. Oceanic Technol.*, *26*(11), 2310–2323.

Wiscombe, W. J., and S. G. Warren (1980), A model for the spectral albedo of snow. i: Pure snow, *J. Atmos. Sci.*, *37*(12), 2712–2733.

Wooster, M. J., G. Roberts, G. L. W. Perry, and Y. J. Kaufman (2005), Retrieval of biomass combustion rates and totals from fire radiative power observations: Frp derivation and calibration relationships between biomass consumption and fire radiative energy release, *J. Geophys. Res. Atmos.*, *110*(D24), n/a–n/a, d24311.

Zaveri, R. A., R. C. Easter, J. D. Fast, and L. K. Peters (2008), Model for Simulating Aerosol Interactions and Chemistry (MOSAIC), *J. Geophys. Res. Atmos.*, *113*(D13), D13204.